



**Queensland University of Technology**  
Brisbane Australia

This is the author's version of a work that was submitted/accepted for publication in the following source:

Jiao, Yalong, Ma, Fengxian, Gao, Guoping, Bell, John, Frauenheim, Thomas, & Du, Aijun  
(2015)

Versatile single-layer sodium phosphidostannate(II): Strain-tunable electronic structure, excellent mechanical flexibility, and an ideal gap for photovoltaics.

*The Journal of Physical Chemistry Letters*, 6, pp. 2682-2687.

This file was downloaded from: <http://eprints.qut.edu.au/85134/>

© Copyright © 2015 American Chemical Society

**Notice:** *Changes introduced as a result of publishing processes such as copy-editing and formatting may not be reflected in this document. For a definitive version of this work, please refer to the published source:*

<http://doi.org/10.1021/acs.jpcllett.5b01136>

# Versatile Single-layer Sodium Phosphidostannate(II): Strain-tunable Electronic Structure, Excellent Mechanical Flexibility and an Ideal Gap for Photovoltaics

*Yalong Jiao<sup>1</sup>, Fengxian Ma<sup>1</sup>, Guoping Gao<sup>1</sup>, John Bell<sup>1</sup>, Thomas Frauenheim<sup>2</sup> and Aijun Du<sup>1,\*</sup>*

<sup>1</sup>School of Chemistry, Physics and Mechanical Engineering Faculty, Queensland University of Technology, Garden Point Campus, QLD 4001, Brisbane, Australia

<sup>2</sup>Bremen Center for Computational Materials Science, University of Bremen, Am Falturm 1, 28359 Bremen, Germany

## Abstract

As layered materials always exhibit new intriguing electronic properties, the search for new types of two-dimensional (2D) monolayers is of significance for next generation miniature electronic and optoelectronic device fabrication. In this work, density functional theory (DFT) calculations were performed to study the structural, mechanical, electrical, optical properties and strain effects in single-layer sodium Phosphidostannate(II) (NaSnP). We find that the exfoliation of single-layer NaSnP from bulk form is highly feasible since the cleavage energy is comparable to graphite and molybdenum disulphide (MoS<sub>2</sub>). The calculated phonon spectrum is free from imaginary frequencies, suggesting single-layer NaSnP is dynamically stable. In addition, the breaking strain of NaSnP monolayer is comparable to other widely studied 2D materials including MoS<sub>2</sub> and graphene, indicating excellent mechanical flexibility of 2D NaSnP. At the level of hybrid functional method, the calculated band gap of single-layer NaSnP is close to the ideal band gap of solar cell materials (1.5eV), demonstrating great potential in future photovoltaic application. Furthermore, strain effect study shows that a moderate compression (2%) can trigger indirect-to-direct gap transition, which would enhance the ability of light absorption for NaSnP monolayer. With sufficient compression (8%), the single-layer NaSnP can be tuned from semiconductor to metal, suggesting great applications in nanoelectronic devices based on strain engineering techniques.

## Introduction

Layered materials in their bulk forms have been well known and utilized in device application for hundreds of years. For instance, graphite has been extensively used in industry for steel-making, as brake lining or as dry lubricant owing to their layered nature, since atoms are strongly bonded in-plane but weakly interact out-of-plane through van der Waals forces. This weak interlayer interaction makes it possible to extract one or a few layers from their bulk forms, leading to the progress in exfoliation techniques such as micromechanical cleavage,<sup>1</sup> surfactant-assisted ultrasonication<sup>2</sup> and liquid Exfoliation<sup>3</sup>. These methods have laid the foundations for the manufacture of essentially any given layered bulk material in the monolayer limit,<sup>3,4</sup> hence opening the ways for burgeoning research on two-dimensional (2D) materials.<sup>5,6</sup>

Compared with traditional 3D photonic materials such as gallium arsenide (GaAs) and silicon (Si), 2D materials exhibit many exceptional properties. First, the confinement of charge and heat transport to the 2D plane leads to a wealth of unusual electronic and optical properties that are distinctively different from their bulk counterparts.<sup>7,8</sup> For example, despite being atomically thin, some 2D materials such as MoS<sub>2</sub> absorb much higher vertically incident light than their bulk forms.<sup>9</sup> Second, 2D materials are easy to integrate into photonic structures such as waveguides<sup>10,11</sup> as their surfaces are naturally passivated without any dangling bonds. Third, conventional 'lattice mismatch' issues can be ignored when constructing vertical heterostructures<sup>12</sup> using different 2D materials, since layers with differing lattice constants are only weakly attached by van der Waals force in heterostructures, structurally similar to that in layered bulk materials.

Up to now, a diverse range of intriguing properties for 2D materials have been revealed, highlighting great potential applications in energy,<sup>13</sup> photonics<sup>14</sup> and nanoelectronics.<sup>15,16</sup> However, the existing 2D materials, in practical, are still very limited because they always suffer from some serious problems such as bandgap hurdles, i.e., the lack of obvious gap in graphene<sup>17,18</sup> and too large gap in hexagonal boron nitride.<sup>19</sup> Although single-layer metal di-chalcogenide such as MoS<sub>2</sub> has a relatively appropriate band gap<sup>8</sup>, they are strongly affected by metal contacts,<sup>20</sup> interface traps,<sup>21</sup> charged impurities,<sup>22</sup> dielectric environment,<sup>23</sup> and structural defect.<sup>24</sup> Under this context, the search for new types of 2D structures is of paramount importance for next generation nanodevice fabrication.

As a member of layered-material family and a typical ternary compound, sodium Phosphidostannate(II) (NaSnP) adopts the KSnAs structure type<sup>25</sup> crystallising in the non-centrosymmetric space group P63mc. The NaSnP crystal has been synthesised experimentally for almost two decades.<sup>26</sup> With similar structures, some ternary compounds have been investigated on their unusual electronic and thermoelectric properties.<sup>27,28</sup> But to the best of our knowledge, few

works have been focused on NaSnP both experimentally and theoretically, and the electrical and optical properties of NaSnP bulk and monolayer still remain unknown. In this work, the possibility of NaSnP exfoliation is investigated in detail by the analysis of mechanical cleavage energy and stability. The electrical properties of NaSnP in bulk and monolayer forms are systematically studied at the level of general gradient approximation and hybrid functional. The imaginary dielectric function of NaSnP monolayer is computed and compared with other 2D materials. Furthermore, the strain effects on the bandgap modulation and mechanical properties are investigated in an attempt to tailor the electronic and optical properties of 2D NaSnP for potential applications in novel electronic nanodevices.

## Computational details

First-principles calculations were performed based on the density functional theory (DFT) using the plane-wave basis VASP code.<sup>29,30</sup> The generalized gradient approximation in the Perdew, Burke, and Ernzerhof form (GGA-PBE) was used as exchange correlation functional<sup>31</sup> for the calculations of geometries and band structures of NaSnP. The hybrid density functional theory based on Heyd-Scuseria-Ernzerhof (HSE) exchange correlation functional<sup>32,33</sup> was adopted to calculate the optical absorption spectrum as well as correct the well-known underestimation of band gap in the PBE calculations. A damped van der Waals correction was incorporated using Grimme's scheme<sup>34</sup> to better describe the non-bonding interaction. The projector-augmented-wave (PAW) method<sup>35</sup> were used to describe the electron-ion interaction and the plane-wave energy cutoff was set to 500 eV. To study 2D systems under the periodic boundary condition, a vacuum layer with a thickness at least 15 Å was set to minimize artificial interactions between neighbouring layers. Monkhorst-Pack k-points<sup>36</sup> of 11x11x3 and 11x11x1 were used for sampling in the first Brillouin zone during geometry optimizations of NaSnP bulk and monolayer, respectively. All the atoms have been fully relaxed until residual force and energy were converged to 0.005eV/Å and 10<sup>-6</sup>eV, respectively. Phonon band structure was computed using density-functional perturbation theory (DFPT),<sup>37</sup> as implemented in the Quantum-ESPRESSO package.<sup>38</sup>

## Results and discussion

### 1. Structural properties

The structure of NaSnP crystal (Fig. 1a) is built from puckered graphite-like sheets in which Sn and P occupy alternative position in each six-membered ring. The Na atoms lie over the centers of the

puckered hexagons. Figure 1b and 1c present the top and side views of NaSnP monolayer, respectively. Detailed structural parameters for bulk and monolayer NaSnP are illustrated in Table 1. The lattice constant of single-layer and the bond length of Sn-P are 4.01 and 2.702 Å, slightly larger than those in bulk counterpart (3.90 and 2.619 Å). Overall, the calculated structural parameters of bulk NaSnP are in very good agreement with the experimentally measured values.<sup>26</sup>

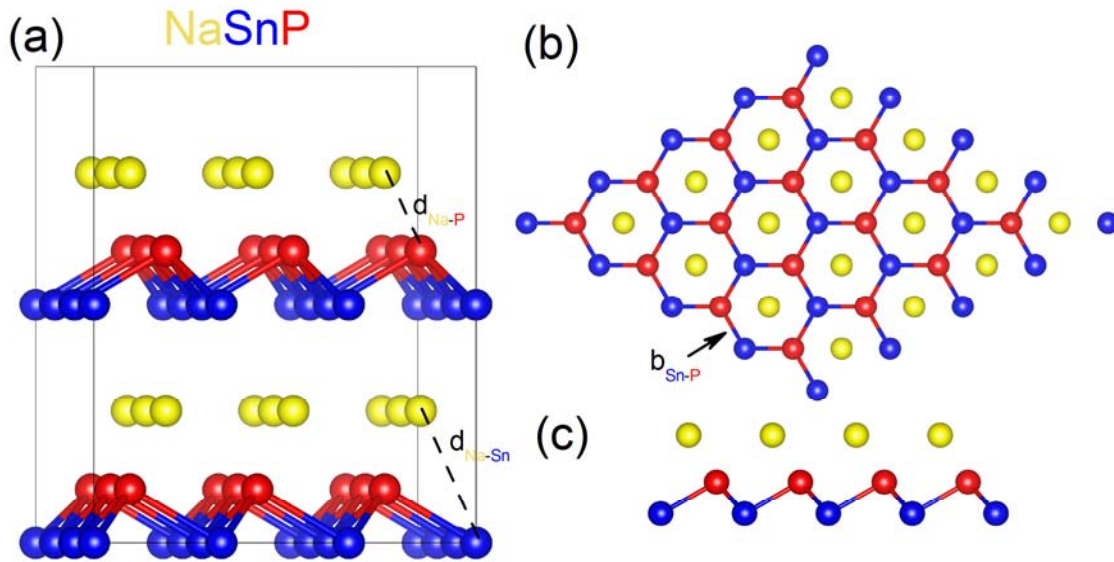


Figure 1. (a) Crystal structure of NaSnP, (b) top and (c) side views of NaSnP monolayer. The yellow, blue and red balls represent sodium, tin and sulfur atoms, respectively.  $d_{\text{Na-P}}$ ,  $d_{\text{Na-Sn}}$  and  $b_{\text{Sn-P}}$  are the Na-P distance, Na-Sn distance and Sn-P band length, respectively.

Table 1. Calculated structural parameters of NaSnP bulk and monolayer using DFT-PBE method. Corresponding experimental values<sup>26</sup> are also given.

	Bulk (Cal.)	Bulk (Exp.)	Monolayer (Cal.)
<b>symmetry</b>	P63mc	P63mc	P3m1
<b>lattice constant (Å)</b>	a=3.90,c= 11.438	a=3.88(2),c= 11.667(2)	a=4.01
<b>bond length <math>b_{\text{Sn-P}}</math>(Å)</b>	2.619	2.596(3)	2.702
<b>Atom distance <math>d_{\text{Na-P}}</math>(Å)</b>	2.933	2.968(4)	2.758
<b>Atom distance <math>d_{\text{Na-Sn}}</math>(Å)</b>	3.369	3.417(4)	3.700
<b>Bond angle(Sn-P-Sn)</b>	96.306°	96.9(1)°	95.968°

## 2. Stability and mechanical properties

To begin with, the possibility of obtaining NaSnP monolayers is estimated using a mechanical exfoliation strategy (Fig. 2a). The cleavage energy  $E_{cl}$  is defined as the minimum energy required during the exfoliation process.<sup>39,40</sup> In order to evaluate the cleavage energy, we calculated the separation of a NaSnP monolayer from a neighbouring trilayer (inset of Fig. 2a). A vacuum layer at least 20 Å is incorporated into the four-layer slab to avoid the artificial interaction between two neighbouring slabs. Figure 2a (blue curve) shows the calculated separation energy  $E_{cl}$  for NaSnP is 0.81 J/m<sup>2</sup>. The theoretical cleavage strength curve is further obtained by taking the derivative of  $E_{cl}$  with respect to the distance. The cleavage strength  $\sigma$  is estimated to be 2.89 GPa. It should be noted that the calculated cleavage energy of NaSnP (0.81 J/m<sup>2</sup>) is smaller than the cleavage energy of Ca<sub>2</sub>N (1.09 J/m<sup>2</sup>)<sup>40</sup> and comparable to the experimentally estimated value of graphite (0.37 J/m<sup>2</sup>)<sup>41</sup>, suggesting the high feasibility to extract 2D NaSnP from bulk in the laboratory.

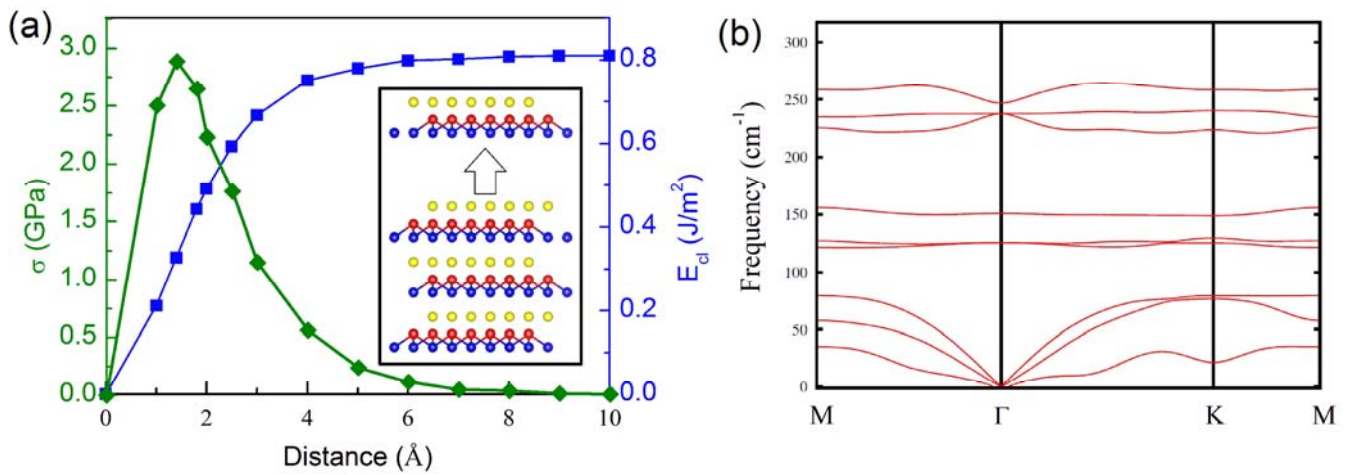


Figure 2. (a) Cleavage energy  $E_{cl}$  in J/m<sup>2</sup> (blue lines) and its derivative  $\sigma$  in GPa (olive lines) as a function of the separation distance  $d$  for a fracture in bulk NaSnP. Inset: Separating a monolayer from its neighboring trilayer. (b) Phonon band structure of NaSnP monolayer along the high-symmetric points in the Brillouin zone.

Then we turn to evaluate the dynamical stability of the NaSnP monolayer by calculating its phonon band structures. There are three atoms in a unit cell, which displays nine phonon dispersion bands as shown in Fig. 2b. It can be clearly seen that no imaginary frequency phonon is found at any wave vector, which confirm the NaSnP monolayer is dynamically stable.

In an attempt to form a freestanding membrane, the NaSnP monolayer must be able to withstand its own weight or external load, which is determined by the in-plane stiffness. It is known that the Young's modulus is a measure of the stiffness of a solid. In the case of NaSnP monolayer, it makes more sense to define the in-plane stiffness ( $Y_{2D}$ ) instead of the classical 3D Young's modulus ( $Y_{3D}$ ), because of the reduced dimensionality of this material. The expression of 2D Young's modulus is

$$Y_{2D} = \frac{1}{S_0} \left( \frac{\partial^2 E_{str}}{\partial \varepsilon^2} \right)_{\varepsilon=0}$$

where  $\varepsilon$  is the axial strain and  $S_0$  is the area of equilibrium surface.  $E_{str}$  is the total strain energy per unit cell defined as  $E_{str} = E_{tot} - E_0$ , where  $E_{tot}$  is the total energy of the strained unit cell,  $E_0$  is the total energy of the strain-free cell. When strain is applied, the system will be disturbed away from the equilibrium state, thus increasing the energy of the system (Fig. 3a). From the strain energy curve in X-axis and the definition of 2D Young's modulus, we find  $Y_{2D} \approx 0.13 \text{ TPa}$ , which is relatively smaller than that of  $\text{MoS}_2$  ( $0.35 \text{ TPa}$ )<sup>42</sup> and graphene ( $1.0 \text{ TPa}$ ).<sup>43</sup> Based on elastic theory, we then test bending of a square NaSnP flake with one edge  $L$  fixed. The out-of-plane deformation  $h$  can be estimated by the expression  $h/L \approx (\rho g L / Y_{2D})^{1/3}$ ,<sup>40</sup> where  $g$  and  $\rho$  represent the gravitational acceleration and the density of the NaSnP monolayer, respectively. For a large NaSnP monolayer flake of length  $L = 50 \mu\text{m}$ , the ratio  $h/L \approx 10^{-4}$ , implying that the NaSnP monolayer is strong enough and able to form a free-standing NaSnP membrane.

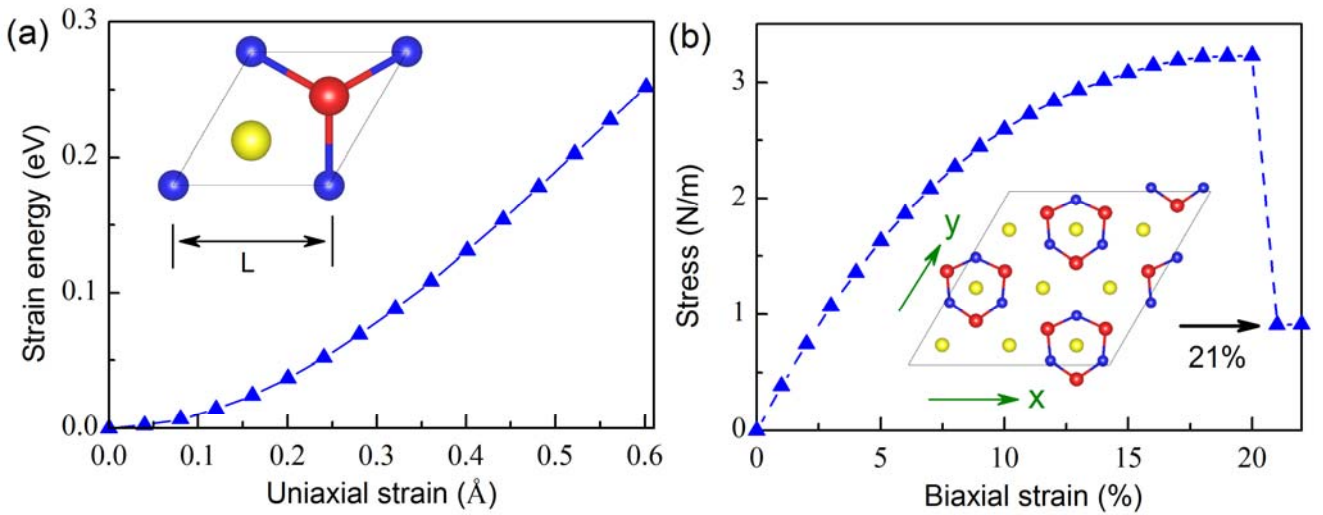


Figure 3. (a) Elastic energy of the NaSnP monolayer under uniaxial strain along x direction. (b) The stress in NaSnP monolayer subjected to biaxial strain. Inset: the structural snapshots under 21% strain. The strain directions are marked by olive arrows.

Next, we estimate the elastic limit of NaSnP monolayer by calculating strain-stress relation subject to a biaxial tensile tension. The maximum stress is the ultimate strength that a material can withstand while being stretched, and the corresponding strain is called ideal strain strength, which is determined by the intrinsic bonding strengths. Beyond the ideal strain strength, the bonds (Sn-P) will eventually rupture as shown in the inset of Fig. 3b. The strain-stress relation in Fig. 3b illustrates that NaSnP monolayer can sustain a stress up to  $3.5 \text{ N/m}$  with the corresponding ideal strain of 20%, which is analogous to that of other well-known 2D materials such as  $\text{MoS}_2$  (20%)<sup>44</sup> and graphene(24%),<sup>45</sup> indicating the high mechanical strength of NaSnP monolayer.

### 3. Electrical properties

Following the studies of the stability and high mechanical strength of NaSnP monolayer, we then turn to investigate its electrical properties. The band structures by the PBE calculations demonstrate that NaSnP bulk (Fig. 4a) is an indirect semiconductor with a band gap of 0.58 eV while the monolayer (Fig. 4a) has a larger indirect fundamental band gap – 1.27eV. The valence band maximum (VBM) of NaSnP monolayer is at the  $\Gamma$  point, and the conduction band (CBM) is at a point along the M–K line. Figure 4c also presents the projected density of state (PDOS) on the atomic orbitals. It can be clearly seen that  $5p$  orbital of Sn and  $3p$  orbital of P demonstrate strong hybridization below Fermi energy. The main contribution above the Fermi energy derives from  $5p$  orbital of Sn,  $3p$  orbital of P and  $5s$  orbital of Sn, and the orbital hybridization effects are still significant.

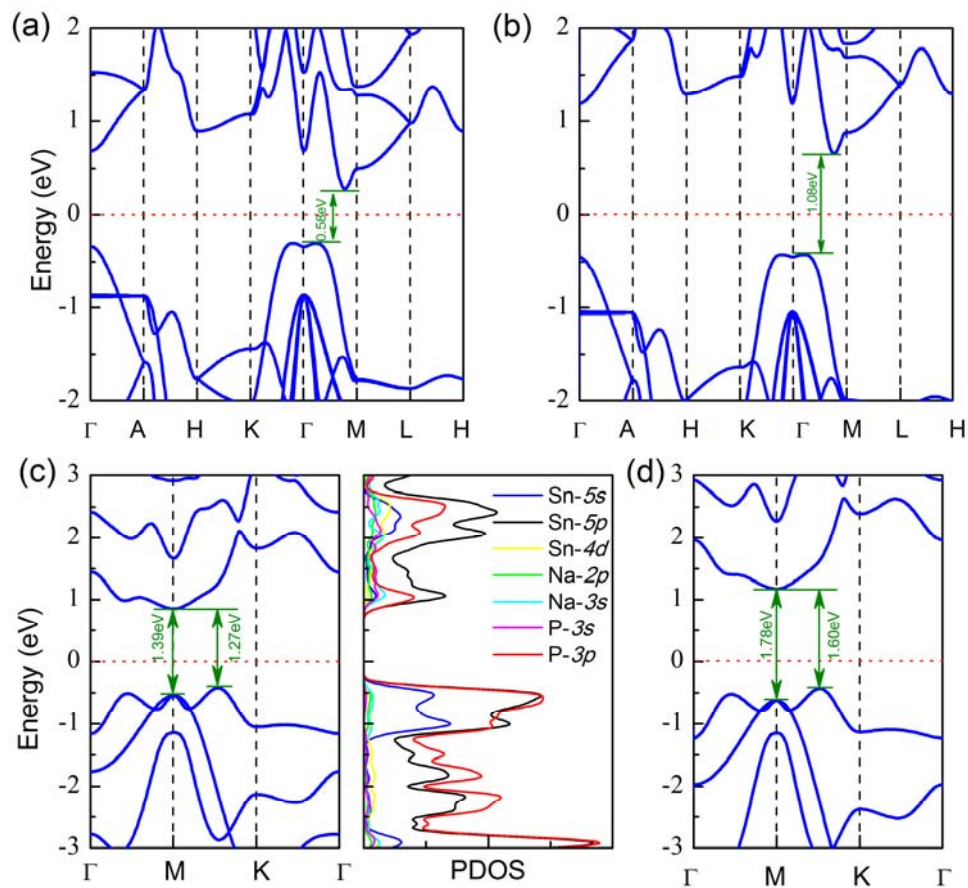


Figure 4. Band structures of NaSnP bulk by (a) PBE (b) HSE06 method; (c) Band structures (left panel) and orbital-projected density of states (right panel) of NaSnP monolayer by PBE method; (d) Band structures of NaSnP monolayer by HSE06 method. The Fermi energy was set to zero.

It is well known that the PBE functional generally underestimates the band gap by about 30%,<sup>46</sup> we therefore perform the hybrid density-functional (HSE06) calculations to obtain more accurate band gap. Our HSE06 calculations correct the indirect band gap of NaSnP bulk and monolayer to 1.08 eV (see Fig. 4b) and 1.60 eV (Fig. 4d), respectively. It should be noted that the fundamental band gap of

NaSnP monolayer is comparable to some high-efficiency photovoltaics materials such as MoS<sub>2</sub> monolayer (1.8eV)<sup>8</sup>, demonstrating the great potential of NaSnP monolayer to form an efficient planar solar cell. The minimum direct band gap (optical band gap) of 2D NaSnP is 1.78eV at M point, which is very close to the ideal optical band gap of solar cell materials (1.5eV). Therefore the 2D NaSnP is expected to possess an excellent performance in harvesting the visible light.

#### 4. Optical properties

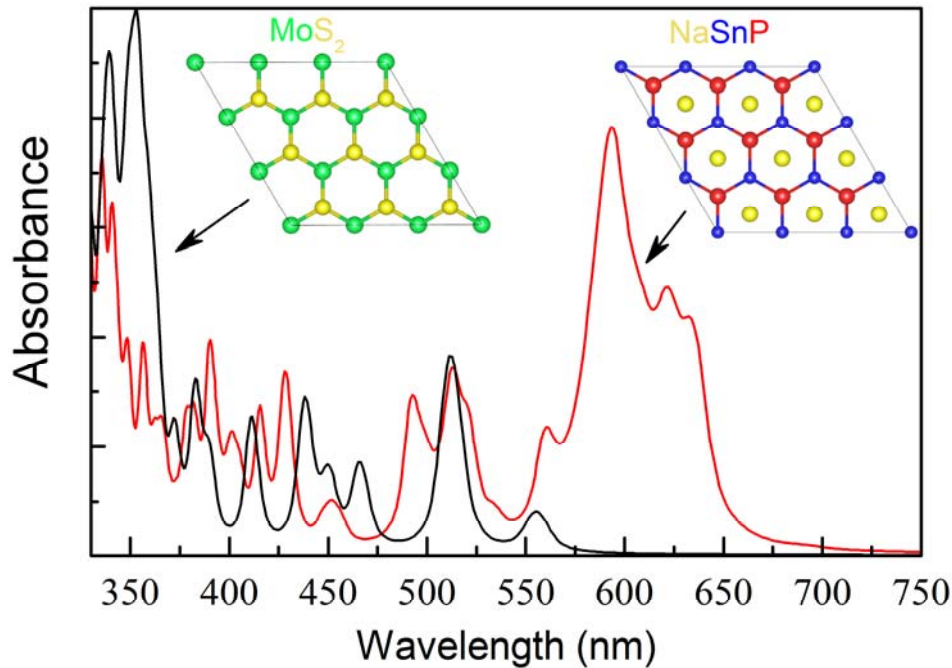


Figure 5. Light absorption spectra of NaSnP (red line) and MoS<sub>2</sub> monolayer (black line) calculated by HSE06 method.

According to the above band gap calculations, single-layer NaSnP should be very active for visible light absorption, which can be confirmed by computing the optical adsorption spectra in visible light region (350nm~700nm) shown in Fig. 5. Results for MoS<sub>2</sub> monolayer, an excellent sunlight absorber, are also included in this Figure for comparison. It can be clearly seen that the MoS<sub>2</sub> monolayer (black line) exhibits high light absorption in short wavelength range, especially at around 350nm, where we can see remarkable absorption peaks. However, it shows low absorption rate at long wavelength end which is partly due to its relatively larger band gap than NaSnP monolayer that hinders the absorption of low frequency (or long wavelength) photons. By contrast, the NaSnP monolayer (red line), with a smaller band gap, has much better optical property at long wavelength region as its predominant absorption peaks locate around 600 nm, and it also shows fairly good light absorption at short wavelength range. Overall the NaSnP monolayer display enhanced visible light response

compared to that of 2D MoS<sub>2</sub>, highlighting potential photovoltaic applications such as being ultra-thin light-absorber.

## 5. Strain effects

NaSnP monolayer is highly polarized materials and strain is expected to tailor its electronic and optical properties. The modulation of band gap and electronic structure by strain would shed new insights on the applications in flexible electronic and photonics devices. Fig. 6 presents the calculated band gap as a function of biaxial strain using the PBE exchange functional. Three strain zones are clearly identified based on the distinct band structure. Zone I is for an indirect band gap with the strain ranging from -2% to 10%, in which the band gap is initially increased and reaches the maximal value of 1.39 eV at 3% strain, then decrease rapidly with further increased expansion. It should be noted that adding a larger strain up to 15% (gap, 0.77eV) is not able to reduce the gap to zero and we find that no band gap transition occurs when 2D NaSnP is stretched. Nevertheless, a moderate -2% compression can trigger this gap transition shown in zone II (-2% ~ -8%), where 2D NaSnP becomes a direct band gap semiconductor, i.e., 1.10 eV under a -2% strain. A further HSE06 calculation corrected this direct band gap to 1.46 eV, which is almost equal to the ideal value (1.5 eV) for solar cell materials, leading to the enhancement of light harvesting at strain = -2%. Most interestingly, the band gap of NaSnP monolayer reduces to zero after the compressive strain reaches -8% and NaSnP monolayer has been turned into a metal as shown in zone III.

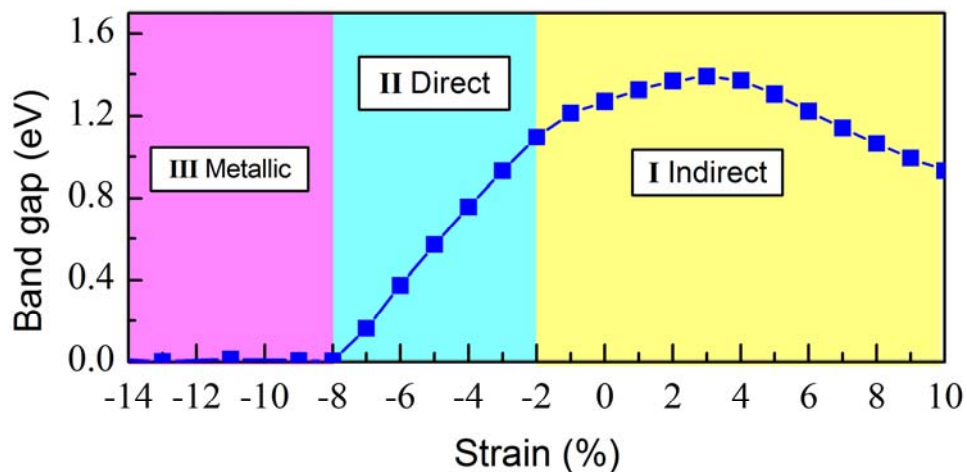


Figure 6. Band gaps of NaSnP monolayer as a function of biaxial strain based on the PBE calculations. Zones I, II and III are corresponding to the indirect band gap, direct band gap and metallic properties, respectively. The critical strains for the gap transitions are -2% and -8%, respectively.

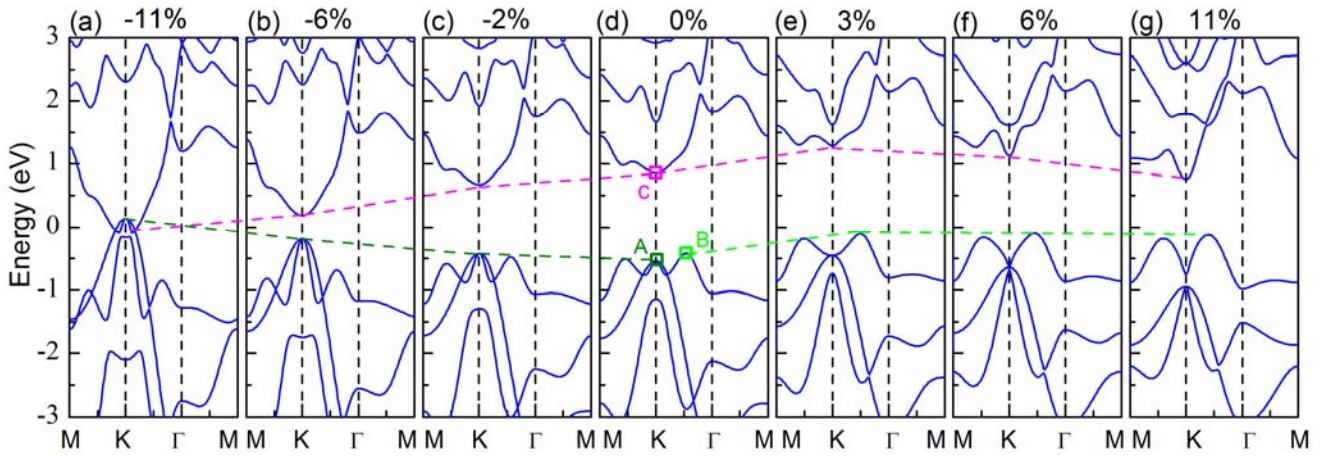


Figure 7. The strain manipulated direct-indirect band gap transition in a 2D NaSnP monolayer. Positive and negative strains correspond to expansion and compression, respectively. The Fermi energy was set to zero.

Figure 7 illustrates that the nature of indirect/direct band gap and semiconductor/metal transition is due to the competition of the energies of several near-band-edge states. For tensile strain (0%~11%), the energy of the conduction band minimum (CBM) labelled as state C in Fig. 7d rises to a maximum at 3% before drops dramatically. By contrast, the energy of the valence band maximum (VBM) at state B (-0.167, 0.333, 0) first slightly increases by 3%, and then keeps almost constant with further expansion. Therefore, the shifts of CBM mainly determine the band gap value under tensile strain. On the other hand, with the increase of compressive strain, the energy of the valence band labelled as state A in Fig. 7d, increases rapidly and becomes higher than that of state B at -2%, indicating an indirect-to-direct gap transition. In addition, both state A and C are shifted toward Fermi level as compressive strain rises, resulting in the significant reduction of band gap. Under -8% strain, the downwards shift of CBM and upwards shift of VBM trigger the semiconductor-to-metal transition. Apparently, the electronic properties of NaSnP monolayer are highly tuneable via applying biaxial strain. In order to maximize the absorption of visible light, a moderate -2% strain in zone II (Fig. 6) is highly desired.

## Conclusion

In summary, we have systematically studied the structural, mechanical, electrical, optical properties and strain effects for NaSnP monolayer. The calculated phonon band structure proves its dynamical stability and the analysis of mechanical properties demonstrate that exfoliation of bulk NaSnP to achieve freestanding monolayers is feasible. The evaluated stress-strain relation indicates that the NaSnP nanosheet is an excellent mechanical material with a breaking strain above 20%. Compared

with MoS<sub>2</sub> monolayer, the band gap value of single-layer NaSnP is closer to the ideal band gap of solar cell materials. Furthermore, optical absorption in a NaSnP monolayer shows enhanced visible-light absorption compared to that of MoS<sub>2</sub>. The strain effects can tune monolayer NaSnP from indirect to direct bandgap and then to metal and, also enhance single-layer NaSnP to be a light absorber. Therefore, NaSnP monolayer could be an excellent material for photovoltaic applications. Further experimental verification is highly desired to develop novel nanoelectronics and photonics device based on NaSnP monolayer.

## Acknowledgements

We acknowledge generous grants of high-performance computer time from computing facility at Queensland University of Technology and Australian National Facility. A.D. greatly appreciates the Australian Research Council QEII Fellowship (DP110101239), financial support of the Australian Research Council under Discovery Project (DP130102420). T. F. and A. D. also acknowledge the financial support (for exchange and visiting) by DAAD/PPPATN57058295.

## Reference

- (1) Novoselov, K. S.; Jiang, D.; Schedin, F.; Booth, T. J.; Khotkevich, V. V.; Morozov, S. V.; Geim, A. K. Two-dimensional atomic crystals. *Proceedings of the National Academy of Sciences of the United States of America* **2005**, *102*, 10451-10453.
- (2) Notley, S. M. Highly Concentrated Aqueous Suspensions of Graphene through Ultrasonic Exfoliation with Continuous Surfactant Addition. *Langmuir* **2012**, *28*, 14110-14113.
- (3) Nicolosi, V.; Chhowalla, M.; Kanatzidis, M. G.; Strano, M. S.; Coleman, J. N. Liquid Exfoliation of Layered Materials. *Science* **2013**, *340*.
- (4) Coleman, J. N.; Lotya, M.; O'Neill, A.; Bergin, S. D.; King, P. J.; Khan, U.; Young, K.; Gaucher, A.; De, S.; Smith, R. J.; Shvets, I. V.; Arora, S. K.; Stanton, G.; Kim, H.-Y.; Lee, K.; Kim, G. T.; Duesberg, G. S.; Hallam, T.; Boland, J. J.; Wang, J. J.; Donegan, J. F.; Grunlan, J. C.; Moriarty, G.; Shmeliov, A.; Nicholls, R. J.; Perkins, J. M.; Grievson, E. M.; Theuwissen, K.; McComb, D. W.; Nellist, P. D.; Nicolosi, V. Two-Dimensional Nanosheets Produced by Liquid Exfoliation of Layered Materials. *Science* **2011**, *331*, 568-571.
- (5) Xia, F.; Mueller, T.; Lin, Y.-m.; Valdes-Garcia, A.; Avouris, P. Ultrafast graphene photodetector. *Nat Nano* **2009**, *4*, 839-843.
- (6) Bonaccorso, F.; Sun, Z.; Hasan, T.; Ferrari, A. C. Graphene photonics and optoelectronics. *Nat Photon* **2010**, *4*, 611-622.
- (7) Novoselov, K. S.; Geim, A. K.; Morozov, S. V.; Jiang, D.; Katsnelson, M. I.; Grigorieva, I. V.; Dubonos, S. V.; Firsov, A. A. Two-dimensional gas of massless Dirac fermions in graphene. *Nature* **2005**, *438*, 197-200.

- (8) Mak, K. F.; Lee, C.; Hone, J.; Shan, J.; Heinz, T. F. Atomically Thin MoS<sub>2</sub>: A New Direct-Gap Semiconductor. *Physical Review Letters* **2010**, *105*, 136805.
- (9) Eda, G.; Maier, S. A. Two-Dimensional Crystals: Managing Light for Optoelectronics. *ACS Nano* **2013**, *7*, 5660-5665.
- (10) Liu, M.; Yin, X.; Ulin-Avila, E.; Geng, B.; Zentgraf, T.; Ju, L.; Wang, F.; Zhang, X. A graphene-based broadband optical modulator. *Nature* **2011**, *474*, 64-67.
- (11) Wang, X.; Cheng, Z.; Xu, K.; Tsang, H. K.; Xu, J.-B. High-responsivity graphene/silicon-heterostructure waveguide photodetectors. *Nat Photon* **2013**, *7*, 888-891.
- (12) Geim, A. K.; Grigorieva, I. V. Van der Waals heterostructures. *Nature* **2013**, *499*, 419-425.
- (13) Jing, Y.; Zhou, Z.; Cabrera, C. R.; Chen, Z. Graphene, inorganic graphene analogs and their composites for lithium ion batteries. *Journal of Materials Chemistry A* **2014**, *2*, 12104-12122.
- (14) Tan, X.; Li, F.; Chen, Z. Metallic BSi<sub>3</sub> Silicene and Its One-Dimensional Derivatives: Unusual Nanomaterials with Planar Aromatic D<sub>6h</sub> Six-Membered Silicon Rings. *The Journal of Physical Chemistry C* **2014**, *118*, 25825-25835.
- (15) Zhang, S.; Yan, Z.; Li, Y.; Chen, Z.; Zeng, H. Atomically Thin Arsenene and Antimonene: Semimetal–Semiconductor and Indirect–Direct Band-Gap Transitions. *Angewandte Chemie International Edition* **2015**, *54*, 3112-3115.
- (16) Kou, L.; Ma, Y.; Tan, X.; Frauenheim, T.; Du, A.; Smith, S. Structural and Electronic Properties of Layered Arsenic and Antimony Arsenide. *The Journal of Physical Chemistry C* **2015**, *119*, 6918-6922.
- (17) Zhou, S. Y.; Gweon, G. H.; Fedorov, A. V.; First, P. N.; de Heer, W. A.; Lee, D. H.; Guinea, F.; Castro Neto, A. H.; Lanzara, A. Substrate-induced bandgap opening in epitaxial graphene. *Nat Mater* **2007**, *6*, 770-775.
- (18) Du, A.; Smith, S. C. Electronic Functionality in Graphene-Based Nanoarchitectures: Discovery and Design via First-Principles Modeling. *The Journal of Physical Chemistry Letters* **2011**, *2*, 73-80.
- (19) Dean, C. R.; Young, A. F.; Merici, L.; Lee, C.; Wang, L.; Sorgenfrei, S.; Watanabe, K.; Taniguchi, T.; Kim, P.; Shepard, K. L.; Hone, J. Boron nitride substrates for high-quality graphene electronics. *Nat Nano* **2010**, *5*, 722-726.
- (20) Das, S.; Chen, H.-Y.; Penumatcha, A. V.; Appenzeller, J. High Performance Multilayer MoS<sub>2</sub> Transistors with Scandium Contacts. *Nano Letters* **2013**, *13*, 100-105.
- (21) Salvatore, G. A.; Münzenrieder, N.; Barraud, C.; Petti, L.; Zysset, C.; Büthe, L.; Ensslin, K.; Tröster, G. Fabrication and Transfer of Flexible Few-Layers MoS<sub>2</sub> Thin Film Transistors to Any Arbitrary Substrate. *ACS Nano* **2013**, *7*, 8809-8815.
- (22) Radisavljevic, B.; Kis, A. Mobility engineering and a metal–insulator transition in monolayer MoS<sub>2</sub>. *Nat Mater* **2013**, *12*, 815-820.
- (23) Sercombe, D.; Schwarz, S.; Pozo-Zamudio, O. D.; Liu, F.; Robinson, B. J.; Chekhovich, E. A.; Tartakovskii, I. I.; Kolosov, O.; Tartakovskii, A. I. Optical investigation of the natural electron doping in thin MoS<sub>2</sub> films deposited on dielectric substrates. *Sci. Rep.* **2013**, *3*.
- (24) Sreepasad, T. S.; Nguyen, P.; Kim, N.; Berry, V. Controlled, Defect-Guided, Metal-Nanoparticle Incorporation onto MoS<sub>2</sub> via Chemical and Microwave Routes: Electrical, Thermal, and Structural Properties. *Nano Letters* **2013**, *13*, 4434-4441.

- (25) Lii, K. H.; Haushalter, R. C. Puckered hexagonal nets in  $2^\infty[\text{Sn}_{33}\text{As}-33]$  and  $2^\infty[\text{Sn}_{33}\text{Sb}-33]$ . *Journal of Solid State Chemistry* **1987**, *67*, 374-378.
- (26) Eisenmann, B.; Rößler, U.: Crystal structure of sodium Phosphidostannate (II),  $\text{NaSnP}$ . In *Zeitschrift für Kristallographie - New Crystal Structures*, 1998; Vol. 213; pp 28.
- (27) Lee, K.; Kaseman, D.; Sen, S.; Hung, I.; Gan, Z.; Gerke, B.; Pöttgen, R.; Feygenson, M.; Neuefeind, J.; Lebedev, O. I.; Kovnir, K. Intricate Short-Range Ordering and Strongly Anisotropic Transport Properties of  $\text{Li}_{1-x}\text{Sn}_2+x\text{As}_2$ . *Journal of the American Chemical Society* **2015**, *137*, 3622-3630.
- (28) Brown, S. R.; Kauzlarich, S. M.; Gascoin, F.; Snyder, G. J.  $\text{Yb}_{14}\text{MnSb}_{11}$ : New High Efficiency Thermoelectric Material for Power Generation. *Chemistry of Materials* **2006**, *18*, 1873-1877.
- (29) Kresse, G.; Furthmüller, J. Efficiency of *ab-initio* total energy calculations for metals and semiconductors using a plane-wave basis set. *Computational Materials Science* **1996**, *6*, 15-50.
- (30) Kresse, G.; Furthmüller, J. Efficient iterative schemes for *ab initio* total-energy calculations using a plane-wave basis set. *Physical Review B* **1996**, *54*, 11169-11186.
- (31) Perdew, J. P.; Burke, K.; Ernzerhof, M. Generalized Gradient Approximation Made Simple. *Physical Review Letters* **1996**, *77*, 3865-3868.
- (32) Heyd, J.; Scuseria, G. E.; Ernzerhof, M. Hybrid functionals based on a screened Coulomb potential. *The Journal of Chemical Physics* **2003**, *118*, 8207-8215.
- (33) Krukau, A. V.; Vydrov, O. A.; Izmaylov, A. F.; Scuseria, G. E. Influence of the exchange screening parameter on the performance of screened hybrid functionals. *The Journal of Chemical Physics* **2006**, *125*, 224106.
- (34) Grimme, S. Semiempirical GGA-type density functional constructed with a long-range dispersion correction. *Journal of Computational Chemistry* **2006**, *27*, 1787-1799.
- (35) Blöchl, P. E. Projector augmented-wave method. *Physical Review B* **1994**, *50*, 17953-17979.
- (36) Monkhorst, H. J.; Pack, J. D. Special points for Brillouin-zone integrations. *Physical Review B* **1976**, *13*, 5188-5192.
- (37) Baroni, S.; de Gironcoli, S.; Dal Corso, A.; Giannozzi, P. Phonons and related crystal properties from density-functional perturbation theory. *Reviews of Modern Physics* **2001**, *73*, 515-562.
- (38) Paolo, G.; Stefano, B.; Nicola, B.; Matteo, C.; Roberto, C.; Carlo, C.; Davide, C.; Guido, L. C.; Matteo, C.; Ismaila, D.; Andrea Dal, C.; Stefano de, G.; Stefano, F.; Guido, F.; Ralph, G.; Uwe, G.; Christos, G.; Anton, K.; Michele, L.; Layla, M.-S.; Nicola, M.; Francesco, M.; Riccardo, M.; Stefano, P.; Alfredo, P.; Lorenzo, P.; Carlo, S.; Sandro, S.; Gabriele, S.; Ari, P. S.; Alexander, S.; Paolo, U.; Renata, M. W. QUANTUM ESPRESSO: a modular and open-source software project for quantum simulations of materials. *Journal of Physics: Condensed Matter* **2009**, *21*, 395502.
- (39) Medvedeva, N. I.; Mryasov, O. N.; Gornostyrev, Y. N.; Novikov, D. L.; Freeman, A. J. First-principles total-energy calculations for planar shear and cleavage decohesion processes in *B* 2-ordered  $\text{NiAl}$  and  $\text{FeAl}$ . *Physical Review B* **1996**, *54*, 13506-13514.
- (40) Zhao, S.; Li, Z.; Yang, J. Obtaining Two-Dimensional Electron Gas in Free Space without Resorting to Electron Doping: An Electride Based Design. *Journal of the American Chemical Society* **2014**, *136*, 13313-13318.
- (41) Zacharia, R.; Ulbricht, H.; Hertel, T. Interlayer cohesive energy of graphite from thermal desorption of polyaromatic hydrocarbons. *Physical Review B* **2004**, *69*, 155406.

- (42) Castellanos-Gomez, A.; Poot, M.; Steele, G. A.; van der Zant, H. S. J.; Agraït, N.; Rubio-Bollinger, G. Elastic Properties of Freely Suspended MoS<sub>2</sub> Nanosheets. *Advanced Materials* **2012**, *24*, 772-775.
- (43) Lee, C.; Wei, X.; Kysar, J. W.; Hone, J. Measurement of the Elastic Properties and Intrinsic Strength of Monolayer Graphene. *Science* **2008**, *321*, 385-388.
- (44) Li, T. Ideal strength and phonon instability in single-layer MoS<sub>2</sub>. *Physical Review B* **2012**, *85*, 235407.
- (45) Bohayra, M.; Gianaurelio, C. Atomistic modeling of mechanical properties of polycrystalline graphene. *Nanotechnology* **2014**, *25*, 215704.
- (46) Xiao, H.; Tahir-Kheli, J.; Goddard, W. A. Accurate Band Gaps for Semiconductors from Density Functional Theory. *The Journal of Physical Chemistry Letters* **2011**, *2*, 212-217.

